Structural Analysis using Landsat TM, Gravity Data, and Paleontological Data from Tertiary Rocks in Yogyakarta, Indonesia

Barianto, Didit Hadi
Department of Earth Resources Engineering, Kyushu University : Doctoral Student

Aboud, Essam
National Research Institute of Astronomy and Geophysics : Geophysicist

Setijadji, Lucas Donny
Geological Engineering Department, Gadjah Mada University : Geologist

Structural Analysis using Landsat TM, Gravity Data, and Paleontological Data from Tertiary Rocks in Yogyakarta, Indonesia

by

Didit Hadi BARIANTO*, Essam ABOUD**

and Lucas Donny SETIJADJI***

Abstract

Herein, we investigate the fault margin that controls the development of the Yogyakarta graben by integrating gravity maps, remote sensing, and foraminifera in Yogyakarta, in the southern part of Central Java, Indonesia. A topographic map was involved to this research to create a shaded map using a Digital Elevation Model (DEM). All data sets were converted into GIS-compatible formats.

Our results indicated that two major faults can be recognized. These major faults divided the area into three parts, including the western, central and eastern parts. The uplift rates of each part were different and created a depressed block control by two parallel faults. Based on foraminifera fossil observations, each block was in the same depositional environment (inner neritic) during N9 (about 14.8–15.1 Ma). The uplift occurred after deposition of marls (Kepek and Upper Sentolo Formations) during the Pliocene, which was then followed by an extension phase since the Pleistocene. The present positions indicate that the western part was uplifted higher than the others, with this part being uplifted more than 590 meters. The central part was uplifted less than 120 meters, and the eastern part was uplifted above an altitude of 170–300 meters.

Keywords: Yogyakarta graben, Gravity maps, Remote sensing, Foraminifera, Fault, Uplift, Pliocene

1. Introduction

The Yogyakarta region is located in the southeastern part of Central Java, Indonesia. The region forms an elongated northeast–southwest-trending central depression bordered by several Tertiary volcanic and carbonate massifs, including (i) the West Progo Mountains to the west (western part), (ii) the Gunung Kidul Mountains to the east (eastern part), (iii) an active Merapi volcano to the north, and (iv) the Indian Ocean to the south (**Fig.1**).

Although this area is physiographically known as a graben[14], all published geologic maps show primarily an eastern normal fault as the border between the central depression and the mountainous zone of the eastern part [19]. In the western part, the location of the fault is unknown. It is possible that the western fault, as the subsurface fault, has been covered by soil and younger sediment. The present study is aimed at determining the location of the fault in the western part of the study area and the relative movements of each block.

* Doctoral Student, Department of Earth Resources Engineering, Kyushu University, Fukuoka, Japan
** Geophysicist, National Research Institute of Astronomy and Geophysics, Cairo, Egypt
*** Geologist, Geological Engineering Department, Gadjah Mada University, Yogyakarta, Indonesia
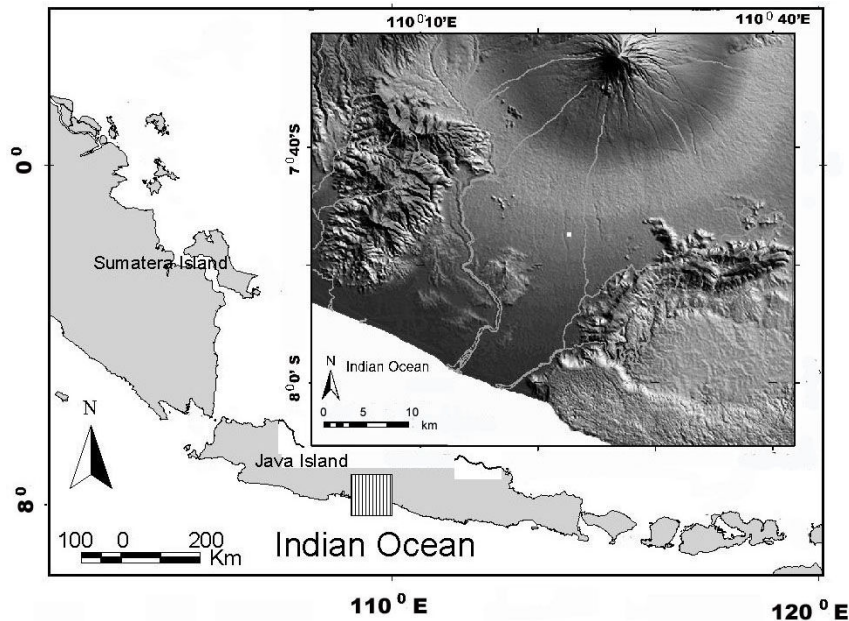
Fig. 1 Location map. Yogyakarta province is located in the southern part of Central Java, Indonesia. Mountainous areas are found in the western and eastern parts and low land areas are found in the central part.

All data sets were converted into GIS-compatible formats. We employed Landsat TM 1995, compiled with height points from topographic maps of Yogyakarta, Indonesia published by BAKOSURTANAL[1] (National Coordinating Agency for Surveys and Mapping, 2001) with a scale of 1: 25,000 for creating 3D images. The edge filter and color shaded map were assembled to extract geological lineaments that were defined as faults and joints using manual interpretation. For subsurface correlations, we used Bouguer anomaly[8], and point data from on-land gravity surveys of Java island compiled by the Geological Research and Development Center in Bandung, Indonesia. The gravity map is technically referred to as a regional gravity map, and contains the Bouguer anomaly on land and the free-air anomaly onshore. Foraminifera were collected at the Jonggrangan Formation, Sentolo Formation, Oyo Formation, Wonosari Formation, and Kepek Formation. All observations were conducted at the Laboratory of Paleontology, Gadjah Mada University, Indonesia. A total of 60 samples were examined in order to identify planktonic and bentonic foraminifera to determine the age and depositional environment of the study area. Fossil observations were identified according to foraminifera biostratigraphy[2,4,5,6,7].

The results of this research revealed that major faults can be recognized on both sides of the study area. The western fault is observed by utilizing horizontal gradient maps and predicted to be a buried fault. This fault is covered by soil and sediment from the Pleistocene marl of the Sentolo Formation and the Quaternary Merapi volcano. Two major faults divide the area into three parts: a western part, a central part, and an eastern part. The uplift rates of each part are different, and based on data from foraminifera fossil observations, each part was at the same level of environmental deposition (inner neritic/ shallow marine) during N9 (about 14.8–15.1 Ma[3]). Currently, the western part is located at an altitude of 590 m above msl (mean sea level), the central part is located at an altitude of less than 120 m above msl, and the Oyo and the eastern part is located above an altitude of 170–300 m above msl. These differences indicate the existence of geological structural boundaries in the form of faults that have different uplifts.

2. The Geological Setting

The West Progo Mountains and the Gunung Kidul Mountains are moderately rugged mountainous areas located in the western and eastern parts of the Yogyakarta region, respectively, and are considered as a

western block and an eastern block. A geologic map of Yogyakarta is shown in **Fig. 2**. Based on reports from Rahadjo et al.[19], the Tertiary rocks unconformably rest upon a metamorphic pre-Tertiary basement (unit 1). The earliest Tertiary rocks are Eocene shallow marine sedimentary rocks that are found as small scattered outcrops at both the Gunung Kidul Mountains (known as the Gamping-Wungkal Formation (unit 2b)) and Kulon Progo Mountains (known as the Nanggulan Formation (unit 2a)). Arc volcanism has been active since the late Oligocene, and most rocks deposited after this period containt some amount of volcanic material. The sediments are overlain by a thick succession of marine volcanics, which represent the late Paleogene volcanic arc (25.4–29.6 Ma[23]) (known as the Gadjah volcanic rocks (unit 3b)). This arc followed an east–west direction, similar to formations found in the western and eastern parts of the region, including the Kebobutak Formation (unit 3a), and the southern part of Nglanggran (unit 3c), including the Parangtritis volcanic rocks   (26.4 and 26.55 Ma[23]).

These rocks are intruded by a diorite-gabbro (unit 4), which then covered volcanic sediments by the early to middle Miocene, namely the Semilir Formation (unit 5), Nglanggran Formation, and Sambiputu Formation (unit 7–8). These rocks are cropped out on the eastern side of the Opak River to form a steep cliff. In the western part, the andesite body was intruded by the Idjo volcanic rocks (unit 6) during the middle Miocene (16.0 to 17.0 Ma[23]).

Volcanic sediment is covered by mixed volcanic and carbonate sediment, known as the Sentolo Formation (unit 9b) in the western part and the Oyo Formation in the eastern part (unit 9a), during the early to late Miocene. Bioturbation, such as animal/worm tracks and trails, have been found in this formation. While the depositional environment of the formations is interpreted to have a deep marine influence, this interpretation remains debatable. In the shallow area, reef growth developed into a carbonate series of the Jonggrangan Formation (unit 10b) in the west and the Wonosari Formation in the east (unit 10a) during the middle to late Miocene. The volcanic region north of Jonggrangan, known as the Menoreh volcanic rocks (unit 10c), developed during the upper Miocene (11.5 and 12.5 Ma[23]).

The Kepek Formation (unit 11a), located in the Gunung Kidul Mountains, was deposited during the late Miocene to Pliocene, which is similar to the upper part of the Sentolo Formation in the west (unit 11b). This formation consists of bedded marls and limestones, which are rich in small foraminifera. In some areas, the Kepek Formation passed laterally into the limestone faces of the Wonosari Formation. The volcanic arc then moved to the north during the Pliocene and deposited volcanic rocks and sediment (unit 12[23]).
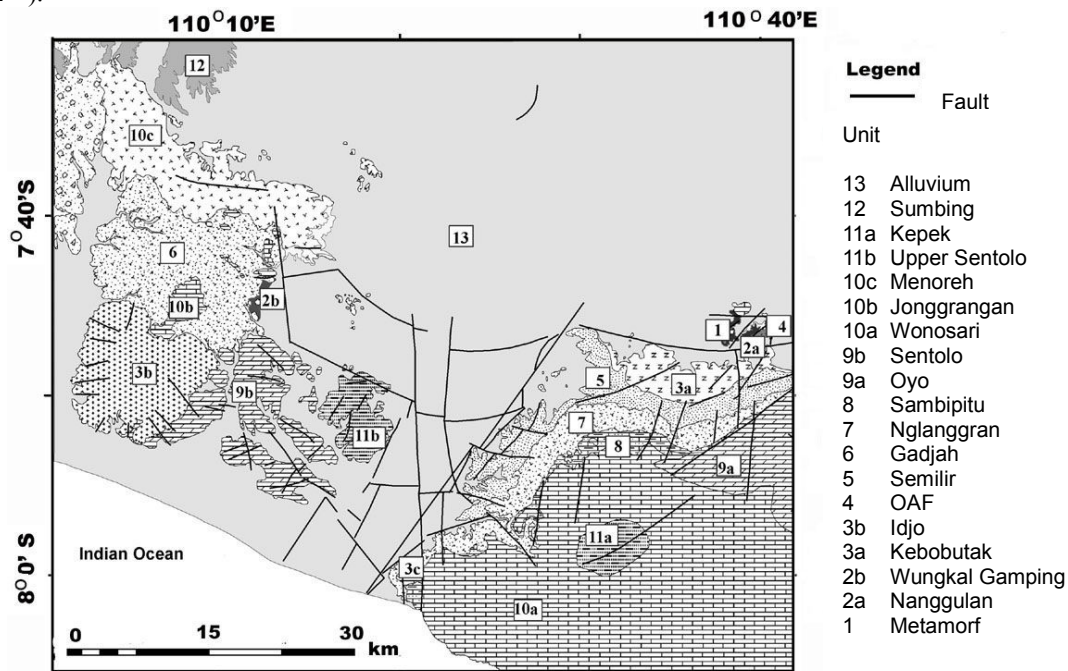

Fig. 2 Geologic Map of Yogyakarta based on Geologic Map 1:100,000 [20], interpretation Landsat TM 1995 and ETM 2001, Topographic Map 1:25,000[1]. Fault data was compiled from previous studies[14, 20, 23, 25].

All of these formations are unconformably covered by Quaternary fluvio-volcanic products of the Merapi and are associated with alluvial deposits (unit 13). The age of the formations is important in order to investigate tectonic evolution by use of lineament maps. All surface expressions are controlled by faults and joints, which occurred after the formation was created.

Four sets of structural trends in the Gunung Kidul Mountains were recognized by previous researcher[25]. They include: (i) the first trend, which is an NE–SW sinistral fault due to N–S compressional stress that was induced by the subduction of the Indo-Australian plate during the late Eocene to late-to-middle Miocene; (ii) the second trend is N–S, and mostly comprised of sinistral faults, except for normal faults at Parangtritis at the western border of the Southern Mountain; (iii) the third trend, which is the NW–SE dextral fault, is the result of the NNW–SSE compressional stress that was developed during the late Pliocene; (iv) the fourth trend, is an E–W, and comprised primarily of normal faults due to an approximate N–S extensional stress during the early Pliocene. This extensional stress has reactivated some pre-existing faults into normal faults.

3.   Data Processing

3.1 Remote sensing

Lineaments were observed from geomorphological criteria based on diagnostic expression of morphotectonics and spectral criteria based on different tones and contrasts [16]. Contrast stretching and edge enhancement filters were applied to Landsat TM in order to improve visual interpretation and emphasize high frequency details to enhance linear features in the image. The intensity of contrast stretching was applied in order to expand the narrow range of brightness values typically present in an input image over a wider range of grey values. The result is an output image designed to accentuate the contrast between features of interest to the image analyst[22]. Edge enhancement filters enhance local discontinuities at the boundaries between different objects (edges). These filters detect edges and either add this back into the original image in order to increase contrast in the vicinity of an edge, or highlight edges using saturated (black, white and color) overlays on the border[13]. An edge represents a discontinuity or sharp change in the grey scale value of a particular pixel at a point, and may be interpreted as a geological structure or relief [15]. The Sobel1 filter was also applied to enhance the linear filter in all directions.

Color-shaded relief maps were established for this research by draping Landsat TM with height point data. The DEM image created the surface from shaded maps by changing the azimuth and elevation of simulated sun illumination to emphasize trends perpendicular and parallel to the sun azimuth. Results from previous studies indicated that the dominant trend of the study area based on field investigations is NE–SW[25]. Therefore, sun illumination coming from the NW–SE was used to avoid an azimuth biasing effect. In addition to other lineament directions, the similar method was conducted in N–S, E–W, and NE–SW directions. All directions have been widely employed for creating shaded maps and extracting geological lineaments in multi trends and angles. The low elevation of sun illumination (30º–45º) was more significant for lineament detection in all directions (**Fig.3**).

The total lineaments extracted from satellite and shaded maps numbered approximately 1,714, with a total length of 1,165 kilometers. These were then divided into four directions, including N–S (447), NE–SW (399), E–W (343), and NW–SE (525), while 121 lineaments were extracted from the geologic map. The dominant trends of joint and fault data, obtained by the field observations of a previous researcher[25], are NW–SE and NE–SW, which are in accord with reported satellite observations. The lineament and fault map can be seen in **Fig. 4**.
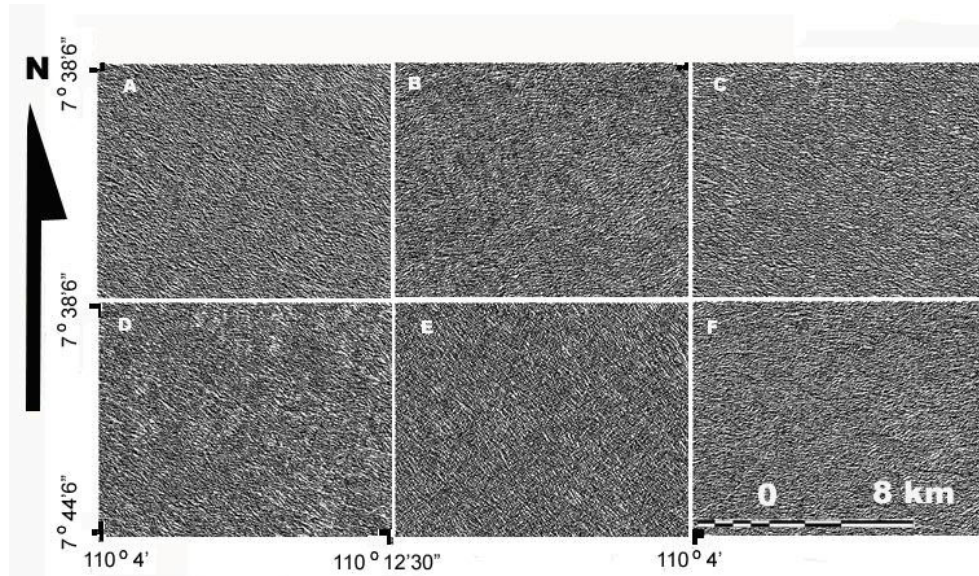
Fig. 3 Partial frame of shaded map shows sun illumination simulation from six directions of similar area. (A) Azimuth NE, elevation 30 °. (B) Azimuth SE, elevation 30 °. (C) Azimuth S, elevation 30 °. (D) Azimuth SW, elevation 45 °. (E) Azimuth W, elevation 45 °. (F) Azimuth NW, elevation 30 °.
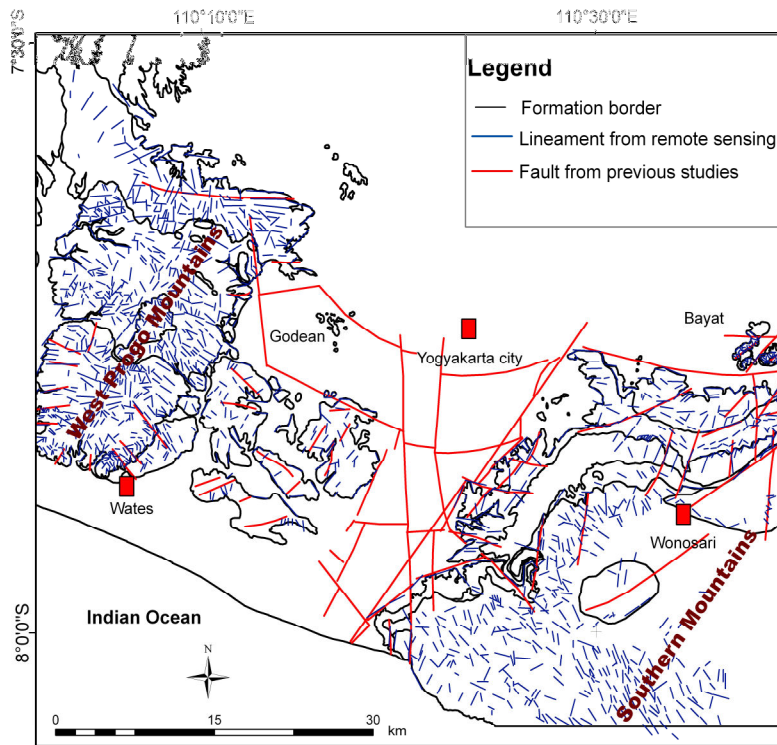

Fig. 4 Lineament map based on Landsat TM image interpretation and fault map data from previous studies[14), 20), 25)].

3.2   Gravity

Gravity data is published as a Gravity Anomaly Map of Western Indonesia with a scale of 1:2,000,000[8)]. The data is sorted according to the study area using GIS extraction clips that result in 470 data points. These points were converted into contours in order to visualize them in 3-D.

The gravity data were employed for making interpretations about subsurface geology in terms of density contrast, which is typically not directly recognized on the surface. Analysis of the gravity data contributes to imaging the subsurface structure of the study area. As such, two filters were used in order to enhance the gravity, including the horizontal gradient filter and the Euler deconvolution.

The horizontal-gradient method has been used since 1982 to locate density/ magnetic boundaries from gravity data or pseudogravity data[9]. The method is based on the principle that a near-vertical fault-like boundary produces a gravity anomaly with a horizontal gradient that is largest directly over the top edge of the boundary. Magnetic data can be transformed to pseudogravity data using Fourier techniques[4], such that they behave like gravity data. Thus, the horizontal gradient of pseudogravity also has a maximum magnitude directly over the boundary. The horizontal gradient contour lines mark the top edges of magnetic or density boundaries.

The horizontal gradient filter provides high values over the faults or contacts. Blakley and Simpson[19] proposed a method to select the highest values of the gridded data at which the faults or contacts are located. Magnetic data can be transformed to pseudogravity data using Fourier techniques[11] such that they behave like gravity data. **Figure 5** shows the horizontal gradient map for the gravity data in the study area. The blue lines represent the boundaries/contacts that were interpreted from the horizontal gradient map. The rose diagram of the blue lines indicates that the dominant direction in the areas is NE–SW.

Euler deconvolution is presented in this study in order to estimate the depths of geological boundaries. Euler deconvolution has come into wide use for automatic estimation of source location and depth. It is particularly useful for determining contacts and estimating their depths. The quality of the depth estimation depends primarily on the choice of the proper structural index (SI) and adequate sampling of the data[27, 12, 26, 17, 10]. Thompson[28], first developed an automated procedure to interpret 2-D magnetic anomalies from Euler's homogeneity equation. Later, Reid et al.,[21] extended this concept to include 3-D magnetic sources. Three-dimensional Euler deconvolution enables large sets of magnetic and/or gravity data over wide study areas to be interpreted rapidly for delineation and depth estimates of different geological structures. The output results are too large to be displayed on the map. In order to select the optimal solutions from the Euler results, an analytic signal was applied to the gravity data. The Euler solution was selected at the location of high values of the analytic signal, as shown in **Fig. 6**.
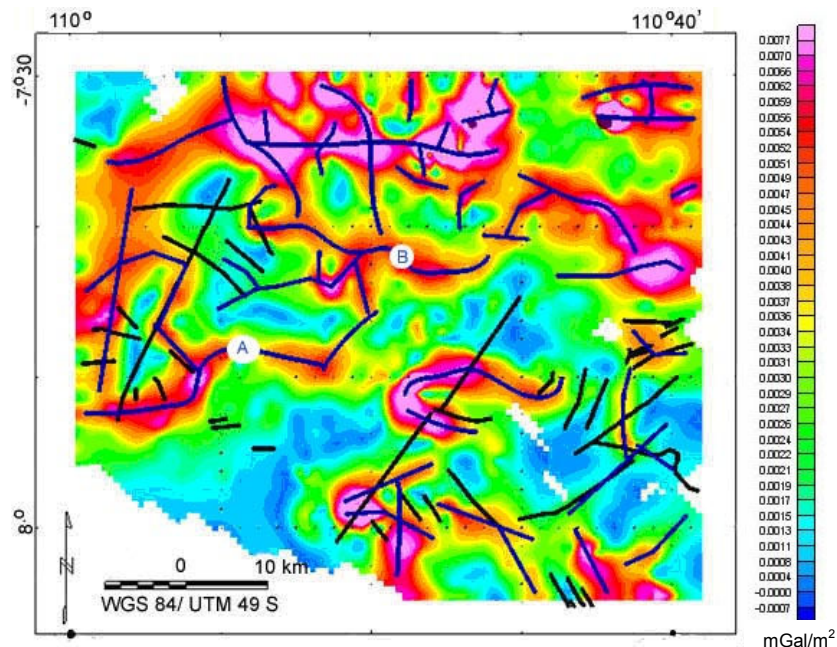

Fig. 5 The horizontal gradient map of the gravity data. Black lines indicate the faults from previous studies[14, 20, 25] and the blue lines show the interpreted faults from the horizontal gradient filter based on the work of Blakely and Simpson[4]. A is the west fault margin and B is E–W fault.

There are similarities between the interpreted lineaments from gravity anomaly maps, the horizontal gradient maps, and the existing geologic maps. The density difference shows the contact between two

different lithologies, which is estimated as a fault if they have a linear contact shape. The use of the gravity map in 3-D (as shown in **Fig. 7**) showed a sedimentary basin trending in the ENE–WSW direction. The result indicates a lineament trending in a NE–SW direction interpreted as a fault, which separates the western block from the central block. This contact is believed to be a fault.

In the western and eastern parts, the Gadjah volcanic rocks and the Nglanggran Formation are exposed beneath the marls of the Sentolo Formation.   The middle part only exposes the Sentolo Formation.   The result of the drilling carried out by Mac Donalds and Partners[1] in the middle part found the same volcanic sediment as that of the Gadjah volcanic rocks and Nglanggran Formation beneath the marls of the Sentolo Formation. This suggests that the middle part was divided by some parallel faults in which the middle is the lowest part relative to all others.
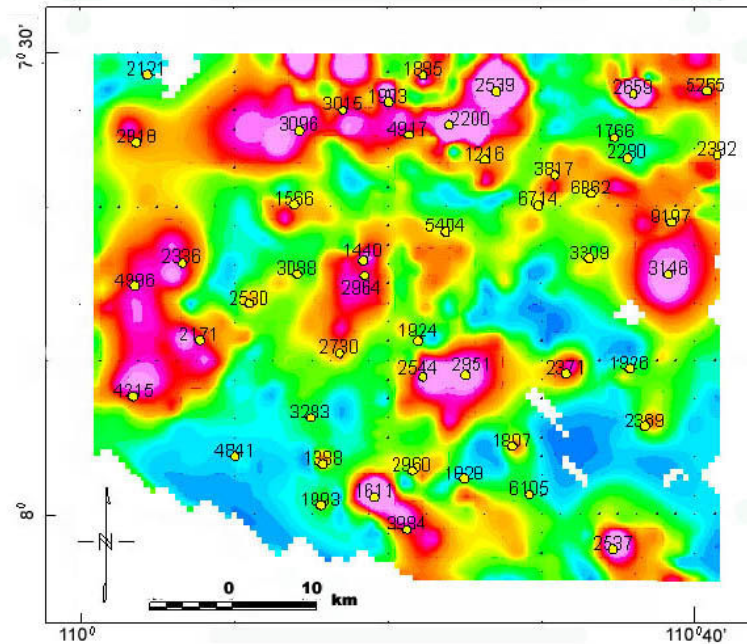

Fig. 6 The analytic signal map of the gravity data (background color map). Euler solutions (open circles) are located at points where the analytical signal gives peaks.
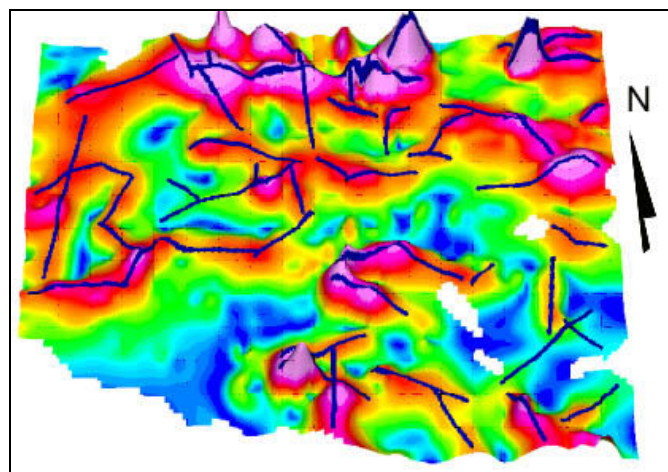

Fig. 7 A 3-D view of the gravity map of the study area. The blue lines show the interpreted faults from the horizontal gradient filter based on the work of Blakely and Simpson[4].

3.3   Fossil

Over sixty samples (primarily limestones and marls) were taken from different locations of four formations, including the Sentolo, Wonosari, Oyo, and Kepek. Cementing material in the samples was removed using water and peroxides. The particles were observed under a binocular microscope with magnifications of 10–100x.

The primary objects of observation were the planktonic and benthonic foraminifera fossils. With reference to Barker[2], Blow[5, 6] and Bolli and Sanders[7], foraminifera fossils can be used to determine the time and environment of sedimentation. Samples used for paleontological analysis were taken from several formations, including the Jonggrangan Formation (in the western part), the Sentolo Formation (in the central part), and the Oyo and Wonosari Formations (in the eastern part). In general, the carbonated sediment in this area was sedimented during the middle Miocene through the upper Miocene, with depositional environments between the inner neritic and the outer neritic environment.

During the middle Miocene (N9), there is a similarity in the sedimentation environments of the four formations. The existence of the planktonic foraminifera such as *Globigerinoides diminutus, Globigerinoides sicanus,* and *Orbulina universa* indicate N9 or during middle Miocene[7]. The existence of the foraminifera bentonic such as *Elphidium advenum*, *Triloculina sp,* and *Amphistegina lessonii* indicate the existence of inner neritic environment[2]. The four formations are currently spread on different height levels, whereby the middle part is in the lowest position (as shown in **Table 1**).   This also shows the possibility of the existence of two faults that bordered the middle part as a normal fault.

In order to predict the uplift time, we observed the fossils of the youngest marine sediments. The youngest marine sediments were found at the top of the mountains, and includes the Kepek Formation and Sentolo Formation. These formations were sedimented during the Pliocene in the outer neritic–upper bathial (100–200 m below sea level). This indicates that from N9 up to the Pliocene, the sedimentation environment becomes deeper. We assume that the uplifting process occured after the Pliocene.

4.   Discussion and Conclusion

There are two origins of geological formations in the present study area from the Tertiary (i.e., the volcanic origin), which are overlain and/or interfingering with a carbonate origin. Both origins were spread widely in the western and eastern parts of the Yogyakarta mountainous area. The central part of Yogyakarta is a low-land area, and consists only of carbonate (interbedded marls and limestone) and Quaternary sediment of Merapi Volcano. Mac Donald and partners[14] , who conducted drilling in the Yogyakarta depression, found volcanic breccia that is similar to the Tertiary volcanic origin, both in the western and eastern parts, beneath carbonate, further suggesting that the depression was controlled by normal parallel faults.

The last published Geologic Map of Yogyakarta showed that the Opak fault is the border of the parallel fault on the eastern margin; however, there is no fault found on the western side. The reason why the western fault remains unknown is that almost no tectonic research has been carried out in this area. Further, there is the possibility that the western fault, as a subsurface fault, has been covered by soil and younger sediment.

Although there are similarities in the geological conditions between the eastern and western parts, they have different lineament densities and trends. Based on remote sensing observations (**Fig. 4**), the expression of lineament control by faulting and jointing in the western part is higher than that in the eastern part. The lineaments that can be found are located predominantly in the western block (897 lineaments), followed by the eastern block (746 lineaments), and then the middle block (71 lineaments). It appears that the expression of lineaments in the western part (which is controlled by higher tectonic activity) is higher than the southern part.

Table 1. Distribution of N9 planktonic foraminifera and their bathymetry. The elevations indicated the west block was uplifted higher than other blocks.

Block	Elevation	Sample No	Zone	Planktonic 1	Planktonic 2	Bathymetry	Bentonic 1	Bentonic 2
West	709 (m)	070808 – 07	N9	*Globigerinoides sicanus*	*Globorotalia peripheroromda*	inner neritic	*Elphidium advenum*	*Nonionella atlantica*
West	630	070808 – 08	N9	*Praeorbulina transitoria*	*Orbulina universa*	inner neritic	*Textularia sp*	*Elphidium advenum*
West	591	070808 – 09	N8	*Globigerinoides sicanus*	*Orbulina universa*	inner neritic	*Elphidium discoidale*	*Triloculina sp*
Central	114	070308-06	N9	*Globigerinoides sicanus*	*Orbulina universa*	outer neritic	*Plamulina faveolata* (Brady)	*Gyroidina soldanii* DOrbigny
Central	113	070308-07	N9	*Orbulina bilobata*	*Globigerinoides diminutus*	outer neritic	*Siphonina pulchra* Cushman	*Cassidulina subglobosa*
Central	70	070810 – 02 B	N9	*Globigerinoides dimminutus*	*Orbulina universa*	middle neritic	*Amphistegina lessonii*	*Robulus sp*
Central	80	070810 – 03	N9	*Orbulina universa*	*Globigerinoides sicanus*	middle neritic	*Amphistegina lessonii*	*Cibicides sp. Aff. C.floridanus*
Central	61	070810 – 05	N9	*Orbulina universa*	*Globigerinoides dimminutus*	inner neritic	*Cassidulina subglobosa*	
Central	63	070810 – 06	N9	*Globigerinoides diminutus*	*Orbulina universa*	inner neritic	*Elphidium advenum*	*Amphistegina lessonii*
Central	73	070810 – 07	N9	*Orbulina universa*	*Globigerinoides dimminutus*	inner neritic	*Ammonia beccarii*	*Amphistegina lessonii*
Central	59	070810 – 09	N9	*Orbulina universa*	*Globigerinoides dimminutus*	middle neritic	*Robulus sp*	*Amphistegina lessoni*
Central	113	060308-10	N9	*Globigerinoides dimminutus*	*Orbulina universa*	outer neritic	*Cassidulina subglobosa*	*Siphonina pulchra*
East	183	070813 – 09	N9	*Globigerinoides sicanus*	*Orbulina universa*	mid neritic	*Amphistegina lessonii*	*Bulimina marginata*
East	352	070814 – 07 A	N9	*Orbulina universa*	*Globigerinoides dimminutus*	inner-mid neritic	*Amphistegina lessonii*	
East	263	070818 – 08	N9	*Globigerinoides sicanus*	*Orbulina universa*	middle neritic	*Amphistegina lessonii*	*Dentalina sp*
East	348	070818 – 22	N9	*Globigerinoides sicanus*	*Orbulina universa*	inner neritic	*Operculina complanata*	*Elphidium advenum* Cushman
East	336	070818 – 20 B	N9	*Globigerinoides sicanus*	*Orbulina universa*	inner neritic	*Amphistegina lessonii*	*Ammonia beccarii*
East	174	070819 – 18	N9	*Orbulina universa* DOrbigny	*Globigerinoides sicamus*	inner-mid neritic	*Amphistegina lessonii*	
East	196	070814 – 11A	N9	*Globigerinoides diminutus*	*Orbulina universa*	inner neritic	*Nodosaria sp*	*Elphidium advenum*
East	198	070814 – 11B	N9	*Globigerinoides diminutus*	*Orbulina universa*	inner-mid neritic	*Amphistegina lessonii*	*Siphonina pulchra*
East	196	070814 – 11C	N9	*Globigerinides diminutus*	*Orbulina universa*	inner neritic	*Cassidulina subglobosa*	*Elphidium advenum*
East	199	070819 -10 A	N9	*Globigerinoides sicamus*	*Praeorbulina transitoria*	middle neritic	*Nodosaria sp*	*Amphistegina lessonii*

The expression of a shear joint can be seen in the Rose diagrams of **Fig. 8, Fig. 9** and **Fig. 10**. N–S (447 lineaments) and NW–SE (525 lineaments) are the dominant trends in this area. Based on the Rose diagram, it appears that tectonic activity from the pre-Oligocene to the upper Miocene was dominated by a compression phase, while the upper Miocene to the Pliocene was dominated by an extension phase. Volcanic evolution of the western block trends from the south (Gadjah volcanic rocks; 25.4–29.6 Ma[24]) to the north (Menoreh volcanic rocks; 11.5 and 12.5 Ma[23]), and was used to analyze the overall tectonic evolution. **Figure 8** indicates that the dominant evolution trends were from NW–SE (Gadjah volcanic rocks), NW–SE and N–S (Idjo volcanic rocks), and E–W (Menoreh volcanic roks), with E–W being the youngest. This result is similar to the regional trend reported by Pulunggono and Mertodjojo[18]. Sudarno[25], reported that the NE–SW, N–S, and NW-SE trends are caused by compression since the Oligocene by NNE–SSW stress, which helped to create the lateral faults. The lineaments in the N–S and NE–SW directions are related to sinistral faults, while the lineaments in the NW–SE direction are related to dextral faults. These faults are related to the compressional phase during the Tertiary. The lineament in the E–W direction is related to normal faults. This fault occurred due to extension since Pleistocene, and also reactivated the N–S and NE–SW sinistral faults as normal faults.
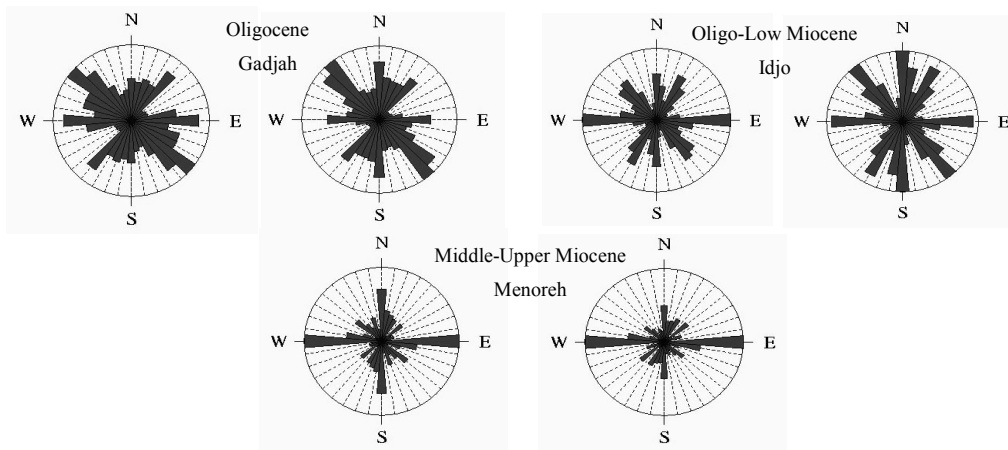

Fig 8. Rose diagrams of the lineament in the western part. The age is derived from geologic formation age based on previous studies[20), 23), 24)].
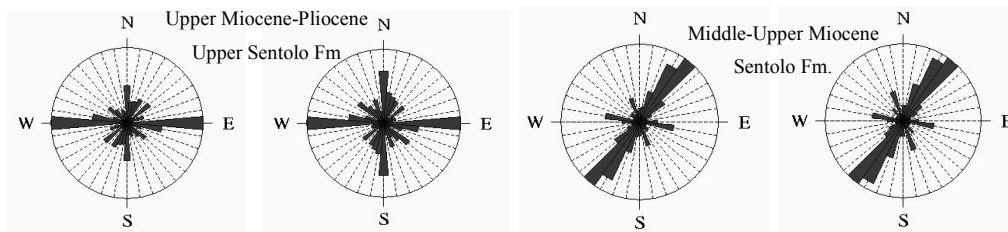

Fig. 9 Rose diagrams of the lineament in central part. The age is derived from geological age data from previous studies [20)] and this research.
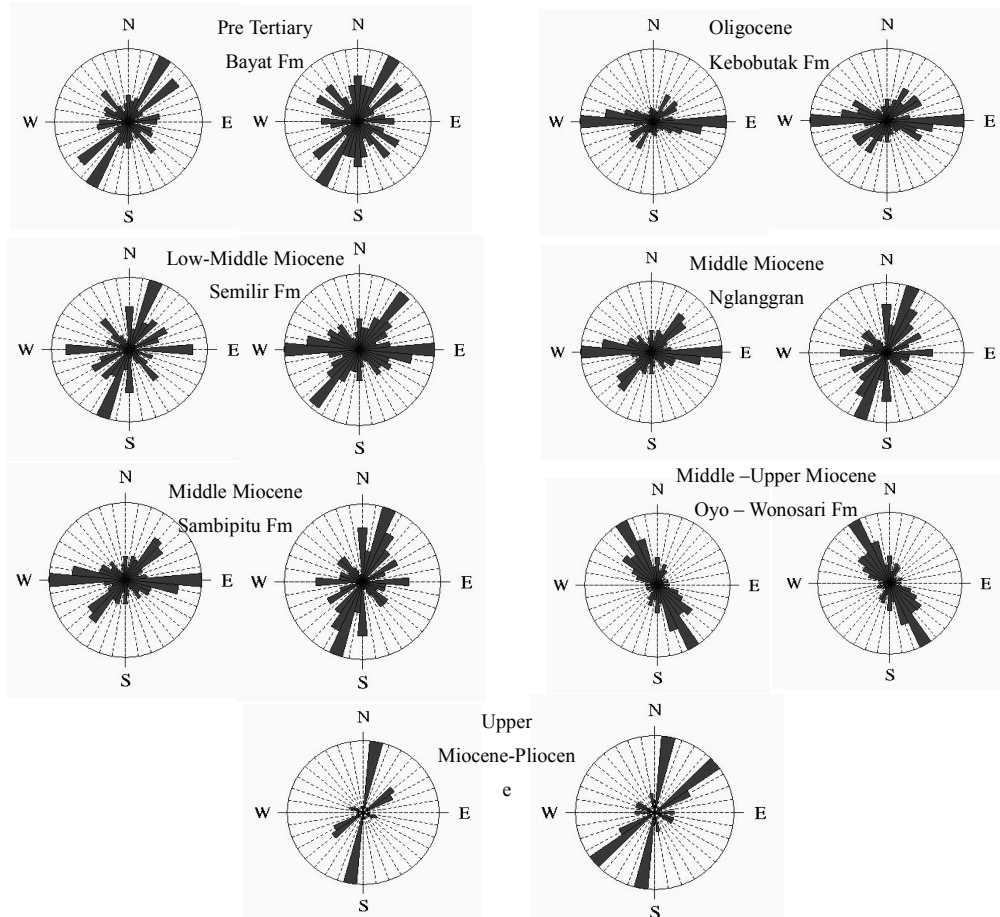
Fig. 10 Rose diagrams of the lineament in the southern part. The age is derived from geological age data from previous studies [20], [23] and this research.

While many lineaments can be observed from satellite images, the existence of the western and northern margins of the graben cannot be seen. Therefore, gravity filters, such as the horizontal gradient, were used to find various faults located in the subsurface. The NE–SW fault as the western margin (A in **Fig. 5**) and the buried E–W fault as the northern margin (B in **Fig. 5**) can be observed. The western margin is controlled by NE–SW, N–S, and E–W faults that stretch up to 45 km from the south to the north. The E–W fault stretches for 55 km from the western part of the Menoreh Mountains to the eastern part of the Kebobutak Mountains. This fault is considered to be a normal fault. This fault occurred due to extension since the upper Miocene[13], which also reactivated the N–S and NE–SW sinistral faults as normal faults.

During the middle Miocene (N9), there was similarity in the sedimentation environments (inner neritic) of the four formations that currently have different elevations (Jonggrangan Formation, i.e. 550 m above msl, Sentolo Formation, i.e. less than 120 m above msl Oyo Formation and Wonosari Formation, i.e. 170–350 m above msl). These differences show the existence of geological structural boundaries in the form of faults that have different uplifts, of which the western block is the highest. They also indicate that the dominant process that has occurred in this area is uplift, rather than the movement of the normal fault. Meanwhile, the tops of the eastern part (Kepek Formation) and the central part (Sentolo Formation) were sedimented at the outer neritic-upper bathial (100–200 m below sea level) during the early Pliocene. Based on this evidence, a major uplift occurred after both formations were created. The distributions of limestones and marls of Jonggrangan, Sentolo, Oyo, Wonosari and Kepek Formations and faults in Yogyakarta graben are shown in **Fig. 11**.

The tectonic history of the Yogyakarta graben during the compressional phase, controlled by NNE–SSW stress during the Tertiary, created the NW–SE and NE–SW lateral faults. The uplift occurred after the late Pliocene, and was then followed by an extensional phase during the Pleistocene. This extension created an E–W normal fault and reactivated a pair of NE–SW sinistral faults as normal faults. These faults are the borders of the Yogyakarta graben.
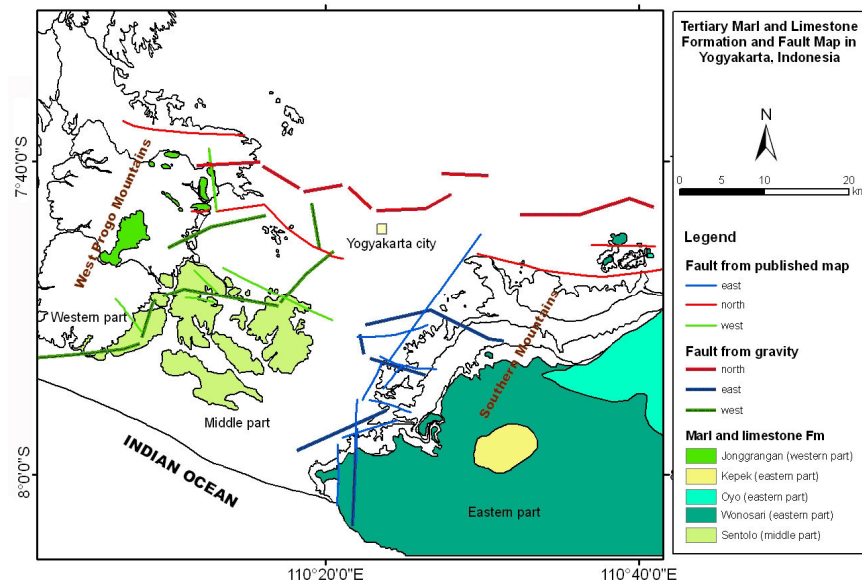
5.   Acknowledgements

Fig. 11 This map shows the fault control development of Yogyakarta graben and distribution of marls and limestone in the study area. The fault was determined based on satellite and gravity data interpretation and fault map data from previous studies[14), 20), 25)] while the marls and limestone distribution was determined based on satellite interpretation.

References

1)   BAKOSURTANAL, Topographic Map Yogyakarta sheet number 1407-1408 (30 sheets), Bakorsurtanal, Bandung (2001).

2)   Barker, R.W.; Taxonomic Notes – on the Species Figured by H. B. Brady in His Report on the Foraminifera Dredged by H.M.S. Challenger during the Years 1873-1876, Society of Economic Paleontologists and Mineralogists, Special Publication No. 9, Tulsa, Oklahoma, 238 p (1960).

3)   Berggren, W.A., Kent, D.V., Swisher III, C.C., Aubry, M.P.; A Revised Cenozoic geochronology and chronostratigraphy. In: Berggren, W.A., et al. (Eds.); Geocronology, Time Scales and Geology, Society of Economic Paleontologist and Mineralogist, Special Publication 54, pp. 129-212, 1995.

4)   Blakely, R. J., and Simpson, R. W.; Approximating edges of source bodies from magnetic or gravity anomalies, Geophysics, v. 51, pp. 1494-1498 (1986).

5)   Blow, W.H.; Late Middle Eocen to Recent Planktonic Foraminiferal Biostratigraphy, Bronnimann, P. and Renz, H.H. eds., Proceedings of The First International Conference on Planktonic Microfossil, Geneva 1967, Leiden, E.J. Brill. Vol. I, (1969).

6)   Blow, W.H., The Cainozoic Globigerinida, Part I and Part II, Section I, Leiden E. J. Brill, New

York, 752 p (1979).

7) Bolli H.M., and Saunders, J.B., Planktonic Stratigraphy, Cambridge University Press, Cambridge, 599 p (1985).

8) Budiman, I., Nasution, J., Sobari, I., and Simamora, W.H., Gravity anomaly map of western part of Indonesia scale 1:2,000,000., Geological Research and Development Centre, Bandung (2000).

9) Cordell, L., and Grauch, V.J.S., Mapping basement magnetization zones from aeromagnetic data in the San Juan Basin, New Mexico, *in* Hinze, W.J., Ed., The Utility of Regional Gravity and Magnetic Anomaly Maps: Soc Explor Geophys, pp.181-197 (1985).

10) FitzGerald, D., Reid, A. and McInerney, P.; New discrimination techniques for Euler deconvolution, 8th SAGA Biennial Technical Meeting and Exhibition, (2003).

11) Hildenbrand, T.G., FFTFIL: A Filtering Program Based on Two –Dimensional Fourier Analysis, U.S. Geol. Surv. Open-file rep. X3-237 (1983).

12) Keating, P.B; Weighted Euler deconvolution of gravity data, Geophysics, v 63, pp. 1595-1603, (1998).

13) Lillesand, T.M. and R.W. Kiefer, Remote sensing and image interpretation, 4th edition, John Wiley & Sons, New York (2000).

14) Mac Donald & Partners (MMP), Greater Yogyakarta groundwater resources study: Volume 3. Groundwater. Technical report for the Directorate General of Water Resources Development Groundwater Development Project, 116 p (1983).

15) Mather P. M., Computer Processing of Remotely - Sensed Images, an introduction, John Wiley & Sons, New York, 352 p (1993).

16) Morelli, M. and F. Piana; Comparison between remote sensed lineaments and geological structures in intensively cultivated hills (Monferatto and Langhe domains, NW Italy), Int. J. Remote Sens., 27, pp. 4471-4493 (2006).

17) Nabighian, M.N. and Hansen, R.O.; Unification of Euler and Werner deconvolution in three dimensions via the generalised Hilbert transform: Geophysics, 66, pp. 1805-1810 (2001).

18) Pulunggono, A., S. Martodjojo; Kerangka tektonik dan stratigrafi Pulau Jawa secara regional dalam kaitannya dengan potensi hidrokarbon, Proceedings Geology and Geoteknik, Jurusan Teknik Geologi UGM, Yogyakarta, pp. 253-274 (1994).

19) Rahardjo, W., Sukandarrumidi, and Rosidi, H.M.D., Geological map of the Jogjakarta Sheet, Jawa. Geological Research and Development Centre, Bandung, 55 p (1977).

20) Rahardjo, W., Sukandarrumidi, and Rosidi, H.M.D., Geological map of the Jogjakarta Sheet, Jawa. 2nd edition, Geological Research and Development Centre, Bandung, 55 p (1996).

21) Reid, A.B., Allsop, J.M., Granser, H., Millett, A.J. & Somerton, I.W.; Magnetic interpretation in three dimensions using Euler deconvolution, Geophysics, v 55, pp. 80-91, (1990).

22) Richard, J.A., Remote sensing digital image analysis, an introduction, 2nd edition, Springer, Berlin (1993).

23) Setijadji, L.D., Geoinformation of island arc magmatism and associated earth resources: a case study from Java Island, Sunda Arc, Indonesia. Doctoral thesis at Kyushu University, Fukuoka, 120 p (2005).

24) Soeria-Atmadja, R., Maury, R. C., Bellon, H., Pringgoprawiro, H., Polves, M., and Priadi, B; Tertiary magmatic belts in Java, Journal of Southeast Asian Earth Science, 9, pp. 13-27 (1994).

25) Sudarno, Ign., Kendali tektonik terhadap pembentukan struktur pada batuan Paleogen dan Neogen di Pegunungan Selatan, Daerah Istimewa Yogyakarta dan sekitarnya. Master Thesis at Bandung Institute of Technology (in Indonesian), 108 p (1997).

26) Silva, J. B. C.,W. E.Medeiros, and V. C. F. Barbosa; Pitfalls in nonlinear inversion, Pure and Applied Geophysics, v 158, pp. 945–964 (2001).

27) Stavrev, P.Y.; Euler deconvolution using differential similarity transformations of gravity or magnetic anomalies, Geophysical Prospecting, v 45, pp. 207-246 (1997).

28) Thompson, D.T.; EULDPH: A new technique for making computer-assisted depth estimates from magnetic data, Geophysics, v 47, pp. 31-37 (1982).